Three-dimensional simulation method of multipactor in microwave components for high-power space application*

Li Yun(李 韵)[a)†], Cui Wan-Zhao(崔万照)[a)], Zhang Na(张 娜)[a)], Wang Xin-Bo(王新波)[a)], Wang Hong-Guang(王洪广)[b)], Li Yong-Dong(李永东)[b)], and Zhang Jian-Feng(张剑锋)[c)]

[a)] *National Key Laboratory of Science and Technology on Space Science, China Academy of Space Technology (Xi'an), Xi'an* 710100, *China*
[b)] *Key Laboratory of Physical Electronics and Devices of the Ministry of Education, Xi'an Jiaotong University, Xi'an* 710049, *China*
[c)] *State Key Laboratory of Millimeter Waves, Southeast University, Nanjing* 210096, *China*

(Received 20 March 2013; revised manuscript received 3 June 2013; published online 10 February 2014)

Based on the particle-in-cell technology and the secondary electron emission theory, a three-dimensional simulation method for multipactor is presented in this paper. By combining the finite difference time domain method and the particle tracing method, such an algorithm is self-consistent and accurate since the interaction between electromagnetic fields and particles is properly modeled. In the time domain aspect, the generation of multipactor can be easily visualized, which makes it possible to gain a deeper insight into the physical mechanism of this effect. In addition to the classic secondary electron emission model, the measured practical secondary electron yield is used, which increases the accuracy of the algorithm. In order to validate the method, the impedance transformer and ridge waveguide filter are studied. By analyzing the evolution of the secondaries obtained by our method, multipactor thresholds of these components are estimated, which show good agreement with the experimental results. Furthermore, the most sensitive positions where multipactor occurs are determined from the phase focusing phenomenon, which is very meaningful for multipactor analysis and design.

Keywords: multipactor, numerical method, three-dimensional, high-power, threshold

PACS: 84.32.–y, 52.40.Db, 79.20.Ap **DOI:** 10.1088/1674-1056/23/4/048402

1. Introduction

With the wide spread of the high-power applications in space, multipactor continues to attract more and more attention in its theoretical, simulation, and experimental study. It is an avalanche of electrons which occurs in low pressure or vacuum environments when certain conditions (frequency, field density, and phase) are met.[1,2] Multipactor discharge can deposit considerable energy in a tiny spot, resulting in power dissipation, performance degradation, surface damage, and even device damages.[3–6] In the past years, multipactor analysis focused on experimental investigations, which is inefficient and expensive. With the development of the computer science, numerical simulation becomes the most economical and essential method. However, due to its complexity and uncertainty, accurate modeling is a challenging task even today. In previous research, the parallel plate approximation was mainly used.[4,7–9] Together with Monte Carlo kinematical motion model,[6–8] the multipactor susceptibility curve developed by the European Space Agency (ESA) was used as a standard by most space industries.[9] Multipactor thresholds obtained from the curve are only reliable for plate structures. Some pioneer work has been done on complex structures, e.g., coaxial lines, elliptical and wedge shaped waveguides analytically.[10–15] The main drawbacks of these studies lie in the high approximation of realistic field distribution and disregarding the electron-field reaction.

Particle-in-cell (PIC) method was first developed to track the electrons in plasma.[16–20] Theoretically, together with computational electromagnetic methods, multipactor effect could be accurately modeled.[21–23] However, due to the high stochastic effect of secondary electron emission and complexity, an efficient and robust three-dimensional algorithm still needs to be further investigated.

Based on the finite-difference time-domain (FDTD) method[24] and PIC method, the self-consistent algorithm which is capable of modeling the interaction between fields and electrons has been proposed first. In order to increase the accuracies of the multipactor thresholds of practical components predicted by our method, the secondary electron emission curve is measured in Section 2. In Sections 3 and 4, the impedance transformer and filter are analyzed by the algorithm, and the numerical results are compared with the experimental data, which show their good agreement.

2. The three-dimensional simulation method for multipactor

Figure 1 shows the flowchart of the three-dimensional (3D) simulation method, which involves the following four main parts:

i) initialization of fields and particles;

*Project supported by the National Key Laboratory Foundation, China (Grant No. 9140C530103110C5301).
†Corresponding author. E-mail: genliyun@126.com
© 2014 Chinese Physical Society and IOP Publishing Ltd

ii) self-consistent algorithm for the field-electron interaction;

iii) modeling secondary electron emission;

iv) prediction of the multipactor threshold.

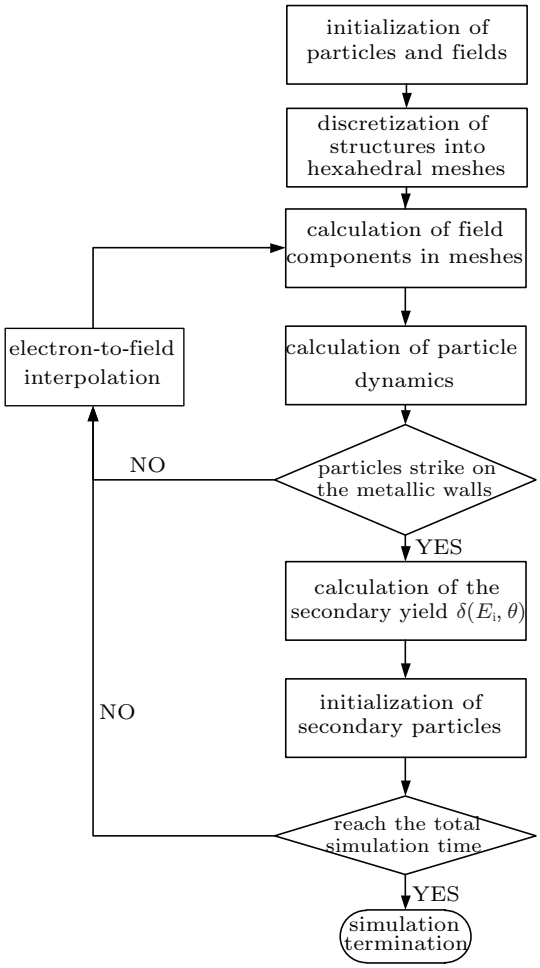


Fig. 1. Simulation flowchart.

2.1. Initialization of fields and particles

Since the FDTD method is adopted, the studied object is first discretized by hexahedral mesh. A macroparticle, rather than the real electrons, is used in the model for numerical consideration.[16,17] The number of electrons contained in the macroparticle is initialized at the very beginning. Besides this, to mimic the real environment in space, a proper number of primary particles should be chosen, which are assumed to be randomly distributed. The kinetic energy and emission angle of the primary particles vary from 0 eV to 10 eV and -90° to 90° respectively (0° refers to the direction normal to the metal surface). The excitation signal is chosen to be sinusoidal, and the frequency and power are set for a given problem. After initialization, the three-dimensional and self-consistent method is used to evaluate the electromagnetic fields and to track and force macroparticles in every cell. Together with the secondary electron emission model, the whole process of multipactor can be recorded. Although the kind of particle can be arbitrary, an electron is assumed to be investigated in this paper for analyzing the multipactor occurring in space.

2.2. Self-consistent algorithm for the field-electron interactions

The motion of an electron under action of the applied fields can be described by Newton-Lorentz equations,

$$\frac{\mathrm{d}}{\mathrm{d}t}mv(t) = q\left[\boldsymbol{E}(\boldsymbol{r},t) + \boldsymbol{v}(t)\times\boldsymbol{B}(\boldsymbol{r},t)\right], \tag{1}$$

$$\frac{\mathrm{d}\boldsymbol{r}(t)}{\mathrm{d}t} = \boldsymbol{v}(t), \tag{2}$$

where m and q denote the mass and charge of the electron, and $\boldsymbol{v}(t)$ and $\boldsymbol{r}(t)$ are the electron velocity and displacement respectively; $\boldsymbol{E}(\boldsymbol{r},t)$ is the electric field intensity; $\boldsymbol{B}(\boldsymbol{r},t)$ is the magnetic induction. Once the electromagnetic fields have been calculated, electron trajectories can be obtained by the PIC method. In most of the previous investigations, effects of electron motion on the fields were ignored for simplification.[10–14] However, it leads to an unacceptable error if the electron number is very huge which is the exact case of multipactor. Consequently, the accurate and self-consistent algorithm are investigated as follows.

As shown in Fig. 2, the electromagnetic fields and electrons are both simulated with the Yee cell,[25] where i, j, and k mean the i-th, j-th, and k-th cells along the x, y, and z axes, respectively. The frog-leaping algorithm resulting from the FDTD method is used to calculate the field distribution. The electron motion is calculated by the discrete differential equations (1) and (2), where the electromagnetic force is obtained through the interpolation of the field components within the same cell. To take into consideration the effects of electron motion on the electromagnetic fields, the electron to field interpolation needs to be formulated.

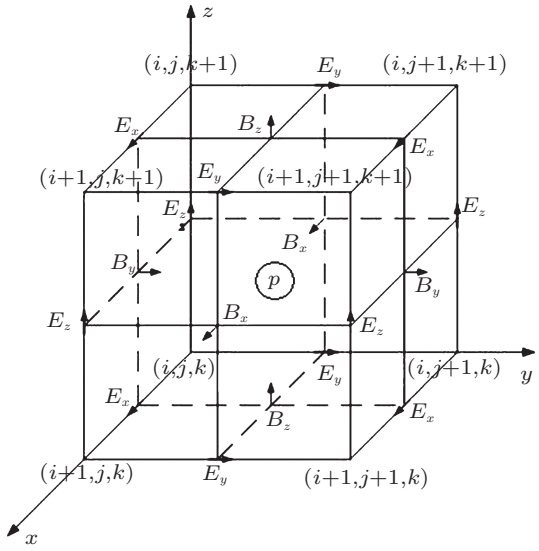


Fig. 2. Fields and electrons in the Yee cell.

As shown in Fig. 3, electron q moves from the position (i_{q1}, j_{q1}, k_{q1}) to the position (i_{q2}, j_{q2}, k_{q2}) in the cell (i, j, k). Given that $\alpha_1 = i_{q1} - i$, $\beta_1 = j_{q1} - j$, $\gamma_1 = k_{q1} - k$, $\alpha_2 = i_{q2} - i$, $\beta_2 = j_{q2} - j$, $\gamma_2 = k_{q2} - k$, the charges at the nodes changed by the electron are obtained though linear interpolating,

$$\begin{aligned}
\Delta Q_{i,j,k} &= (1-\alpha_l)(1-\beta_l)(1-\gamma_l)q,\\
\Delta Q_{i+1,j,k} &= \alpha_l(1-\beta_l)(1-\gamma_l)q,\\
\Delta Q_{i,j+1,k} &= (1-\alpha_l)\beta_l(1-\gamma_l)q,\\
\Delta Q_{i+1,j+1,k} &= \alpha_l\beta_l(1-\gamma_l)q,\\
\Delta Q_{i,j,k+1} &= (1-\alpha_l)(1-\beta_l)\gamma_l q,\\
\Delta Q_{i+1,j,k+1} &= \alpha_l(1-\beta_l)\gamma_l q,\\
\Delta Q_{i,j+1,k+1} &= (1-\alpha_l)\beta_l\gamma_l q,\\
\Delta Q_{i+1,j+1,k+1} &= \alpha_l\beta_l\gamma_l q,
\end{aligned} \tag{3}$$

where $l = 1$ refers to the starting point of the electron motion, and $l = 2$ represents the end point. As shown in Fig. 3, x_1, x_2, and x_3 are used to define a three-dimensional local coordinate system. Current caused by the electron motion is divided into three components according to the local coordinate system. Using the continuity equation

$$\frac{\partial Q}{\partial t} + \oint \boldsymbol{J} \cdot \mathrm{d}\boldsymbol{s} = 0, \tag{4}$$

current at mesh lines can be obtained. Once the current has been calculated by the PIC method, its effect will be manifested through the source term in Ampere's law of Maxwell equations. Obviously, the field and current are the bridge between the FDTD and PIC method, by which the self-consistent characteristic is realized. Without doubt, the accuracy of the proposed method is much higher and the mechanism behind multipactor in real space applications can be captured.

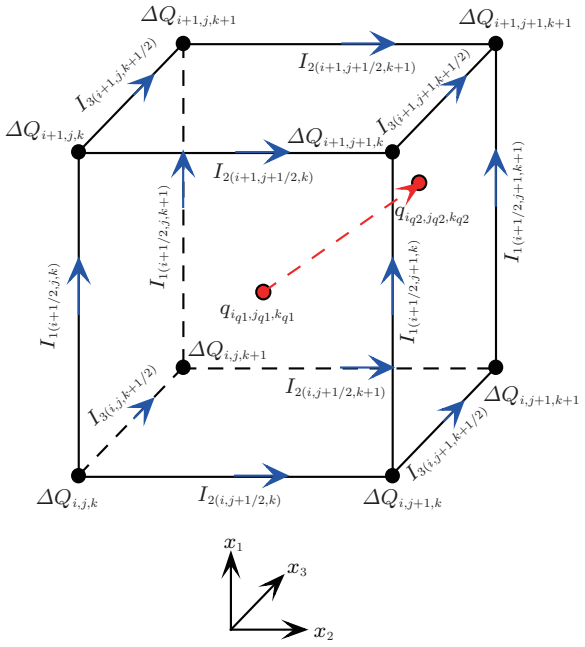


Fig. 3. (color online) Electron-to-field interpolation in Yee cell.

2.3. Secondary electron emission modeling

Secondary electron emission is another key factor to multipactor. Electrons are accelerated between metallic gaps and finally impact on the metal surfaces with a certain energy and angle. Secondary electrons will be knocked out if the collision momentum makes the secondary emission yield (SEY) to be larger than unity. For almost all the metallic materials for space application, the maximum SEYs of them are larger than unity. Then it is a significant risk of multipactor for all the high-power components in space environment.

Depending on the surface contamination, oxidation, sulphide formation, and finishing condition, SEY of the same material may vary to a large extent. In numerical simulation, such variations strongly affect the resulting multipactor threshold. In order to improve the simulation accuracy and make it closer to the practical case, measured SEY for metallic materials is used to model the secondary electron emission.

We construct a system for the measurement of SEY, which is composed of ultra-high vacuum (UHV) chamber, test system, and data processing system as shown in Fig. 4. The test system is composed of a low energy (20 eV–5000 eV) electron gun, ion gun, sample platform, and picoammeter.

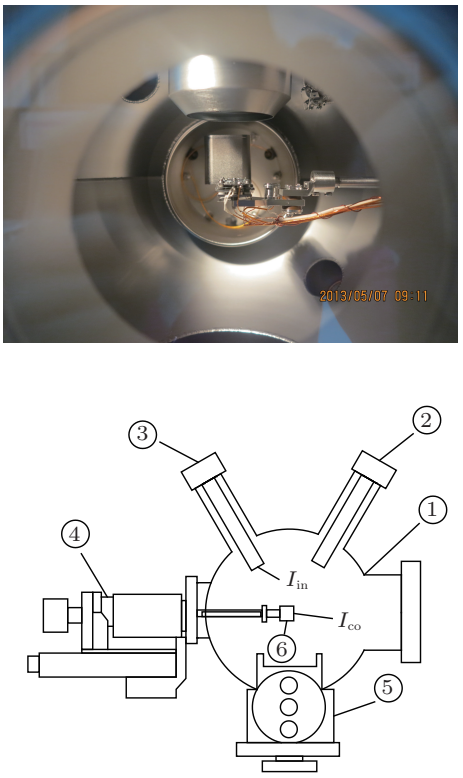


Fig. 4. (color online) SEY measurement system, 1: UHV chamber, 2: ion gun, 3: electron gun, 4: transport system, 5: pumps, 6: sample platform.

The ion gun is used for sample cleaning. SEY is measured with the biased current method[26,27] in the test facility

chamber, where the base vacuum pressure is 10^{-7} Pa. SEY is not measured directly, but calculated by

$$\delta = \frac{I_{\rm in} - I_{\rm co}}{I_{\rm in}}. \tag{5}$$

In the above equation, $I_{\rm in}$ is the incident current on the sample and $I_{\rm co}$ is the collected current.

For numerical simulation, a classic secondary electron emission model was developed by Vaughan.[1] Depending on the electron impacting energy and angle, SEY can be calculated by

$$\delta = \delta_{\max 0}\left(1 + \frac{k_{\rm s}\theta^2}{2\pi}\right)(w{\rm e}^{1-w})^k, \tag{6}$$

$$E_{\max} = E_{\max 0}\left(1 + \frac{k_{\rm s}\theta^2}{2\pi}\right), \tag{7}$$

where

$$w = \frac{E_{\rm i} - E_{\rm threshold}}{E_{\max} - E_{\rm threshold}},$$

$k = 0.62$ for $w < 1$ and $k = 0.25$ when $w > 1$; $k_{\rm s}$ denotes the surface roughness; $\delta_{\max 0}$ and $E_{\max 0}$ are the characteristic parameters of the secondary electron emission properties of certain material; $E_{\rm threshold}$ is a fitting parameter and the model does not work when the impact energy is lower than this value.

As shown in Fig. 5(a), test samples plated with several-μm thick silver have been processed. SEY measurements are performed on them and measured data for the perpendicular incidence case are shown in Fig. 5(b). By classic fitting method, input parameters of the model, including $\delta_{\max 0}$, $E_{\max 0}$, and $E_{\rm threshold}$, can be extracted out of the measured data. Parameters are chosen to guarantee a good match in the low energy range, especially in adjacent to the first cross energy. This fitting criterion is due to the fact that the first cross energy affects multipactor threshold more strongly.[9] The values of $\delta_{\max 0}$, $E_{\max 0}$, and $E_{\rm threshold}$ are fitted to be 2.08, 380, and 10. According to the plating thickness and finishing condition, $k_{\rm s}$ is set to be 1. From Eqs. (6) and (7), the SEY curve is calculated and shown in Fig. 5(b). Comparison with the measured data shows that the fitting error mainly exists in the high energy range and the total root mean square error (RMSE) is less than 0.10. For an arbitrary incident angle, SEY can be obtained through interpolation, thus the fitting model can be used for multipactor simulation.

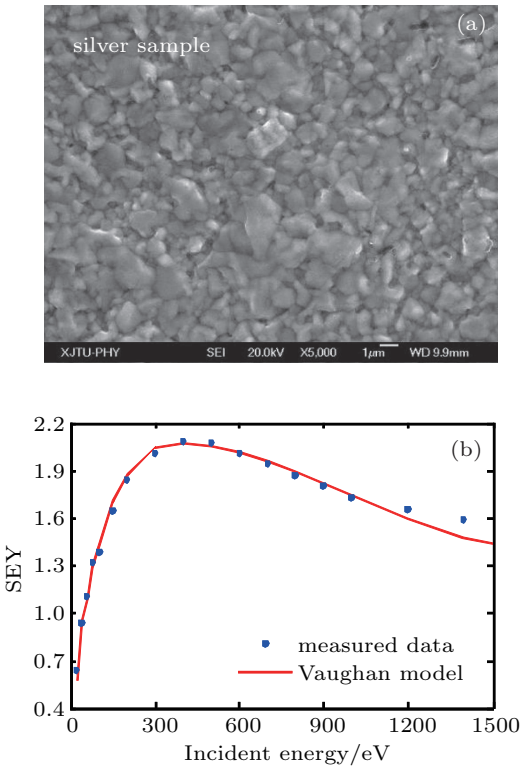


Fig. 5. (color online) (a) SEM image and (b) comparison between the measured SEY curve and the calculated one from fitting model for silver sample.

2.4. Prediction of the multipactor threshold

In the multipactor simulation, after the initialization of the primary electrons and fields, electrons are motivated by the self-consistent algorithm and move in the meshed structure until impact on the metallic walls. Upon impact, secondary electrons are knocked out from the metallic materials. If the number of the secondary electrons is always larger than that of the absorbed one, the avalanche of electrons occurs. As time goes by, the electron avalanche finally induces the multipactor discharge. Consequently, the whole physical process of multipactor is characterized and modeled successfully with our simulation method.

Compared with the analytical means[11–14] or other simulation methods, e.g., multipactor calculator,[9] our simulation method has a remarkable advantage for the threshold prediction. In the simulation process, the number of the electrons at each time step can be recorded. By analyzing the tendency of the transient evolution of this number, the multipactor threshold can be found conveniently, which will be detailed in the next section.

3. Simulation results and discussion

In this section, in order to validate our simulation method, typical microwave components with non-resonant or resonant structures are studied. Some key points in the simulations are discussed in detail.

3.1. Non-resonant impedance transformer

Figure 6 shows the three-dimensional symmetric model of a five-order waveguide impedance transformer. The transformer is plated with silver. The lateral dimension is 29.08 mm, and the longitudinal dimensions are 29.08 mm,

19 mm, 12 mm, 3 mm, and 1 mm respectively. The excited frequency is 3.85 GHz and the working mode is TE_{10} mode. The structure represents the vacuum space in the transformer. The narrowest segment is the loading region of initial macroparticles, each of which contains 100 electrons and they are distributed randomly. The model is then discretized into hexahedral elements with 20 meshes per wavelength. We emphasize that the narrowest gap should be meshed at least by 3 cells in order to guarantee the computational accuracy.

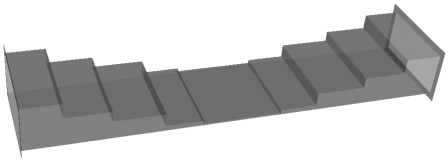


Fig. 6. Impedance transformer.

3.2. Ridge waveguide filter

To further study the capability of our method, the ridge waveguide filter which is a highly resonant and complex component is considered. As shown in Fig. 7(a), the structure is plated with silver and the primary particles are distributed randomly in the vacuum space. The input and output ports are both standard WR229 waveguide ports. Dimensions of the structure are shown in Fig. 7(b) and the unit is millimeters. The excited frequency is 3.9 GHz and the working mode is TE_{10} mode.

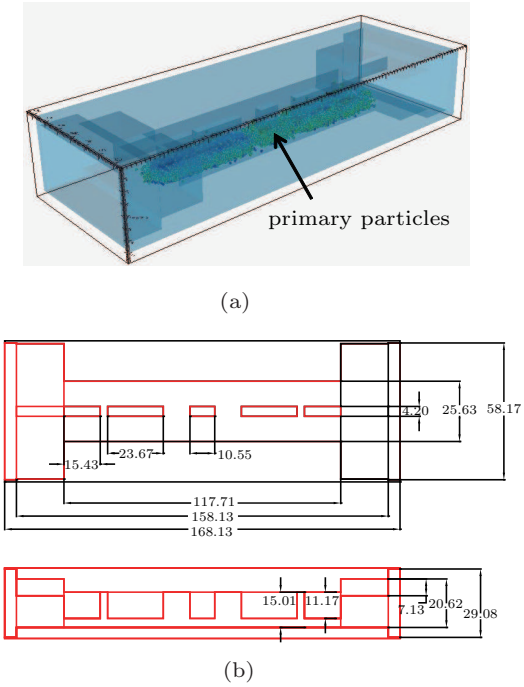


Fig. 7. (color online) Ridge waveguide filter: (a) model, (b) dimensions.

3.3. Results and discussion

Due to the discontinuities in the transformer, high order modes will be excited. It is reasonable to allocate the initial electrons in the narrowest segment since it is the most susceptive region for multipactor occurring due to the strongest field density. Figure 8 shows the interaction between the electrons and the fields. The contour lines denote the field distribution and the points denote the macroparticles.

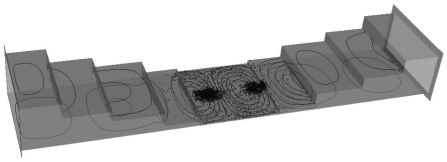


Fig. 8. Interaction between electrons and fields.

Since the presented method is three-dimensional, self-consistent and of time-domain, the physical process of the multipactor generation can be captured and visualized as shown in Fig. 9. From these pictures, the phase focusing effect[4] and the resonant steady state of multipactor are clearly observed. In practice, with time increasing, only the particles which synchronize with the electromagnetic fields can be clustered. Other electrons diffuse rapidly in the components and will be absorbed by the metal walls finally. Thus, the clustered electrons will grow exponentially if the input power is so high that it makes the impact energy of electrons large enough to knock out more secondary electrons.

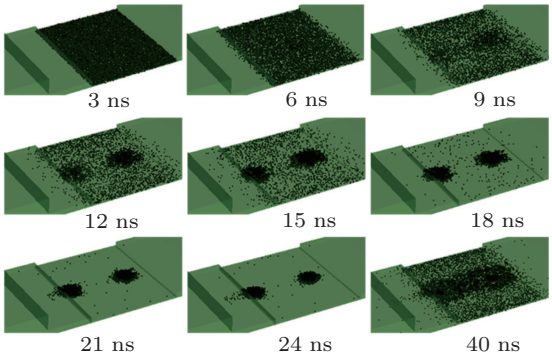


Fig. 9. (color online) Evolution of multipactor in the transformer.

It is deduced that the multipactor discharge breakdown will occur in the transformer at such input power levels. By analyzing the electromagnetic field distribution, we conclude that the electric field intensity in the place where multipactor occurred tends to be the maximum within the transform. Obviously, such places are usually the narrowest parts of the component.

Figure 10 gives the transient evolutions of particle numbers at different input powers. As depicted in Fig. 10, when the input power is low, particles cannot acquire enough energy to accelerate or to synchronize with the field evolution. As a result, particles will be absorbed by the metal walls and the total particle number will decrease with time. On the contrary, if the input power is high enough, many particles will obtain

proper energy and their traverse time will be close to half an RF cycle. Consequently, secondary particles will be knocked out continuously and the multipactor discharge will finally occur due to the avalanche. From the figure, one clearly sees that the input power of 1750 W is the multipactor threshold of the transformer.

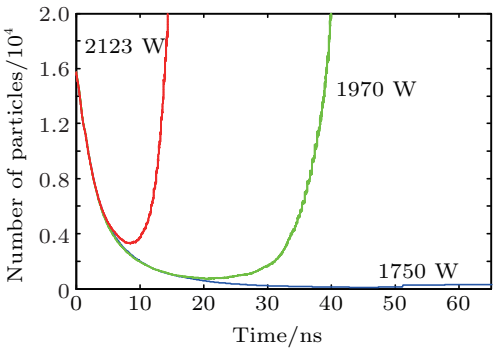


Fig. 10. (color online) Transient evolutions of the particle numbers in the transformer.

Electromagnetic field distribution in the ridge filter is more complex and it is impossible to predefine the susceptive region of multipactor. Thus, initial particles are set to be distributed in the whole simulation domain. One should note that, in order to reduce the computational time, the initial particles have been continuously emitted for about an RF cycle only when the field distribution is steady. Figure 11 shows the transient evolutions of the total particle numbers at different input power levels. As shown, when the input power is 544 W, the particle number keeps increasing for over 200 RF cycles but decreases after 300 RF cycles. According to the classical multipactor theory, the continuous increasing of the electrons seems to be the direct evidence of multipactor discharge, which conflicts with our results. This can be explained by two possible reasons. One is that the initial particles are of great quantity in the interior space of the filter, which need time to diffuse. The other is that due to the complex structure, particles may be clustered in some regions, usually at corners near to the discharge region, for a long time, but these particles will be absorbed finally.

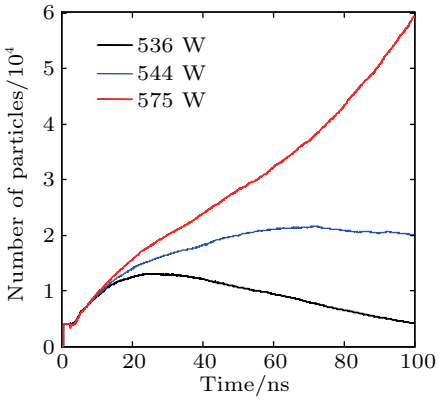


Fig. 11. (color online) Transient evolutions of the particle numbers in the filter.

In order to make it clearer, the transient evolutions of the secondary particle numbers, which exclude the effects of initial particles on the total particle number, are illustrated in Fig. 12. Obviously, the confused phenomenon has been partially alleviated. Essentially, such a phenomenon refers to the nonlinear physics between the electrons and the fields. Thus, it is necessary to take sufficient simulation time to confirm whether multipactor really occurs in the component.

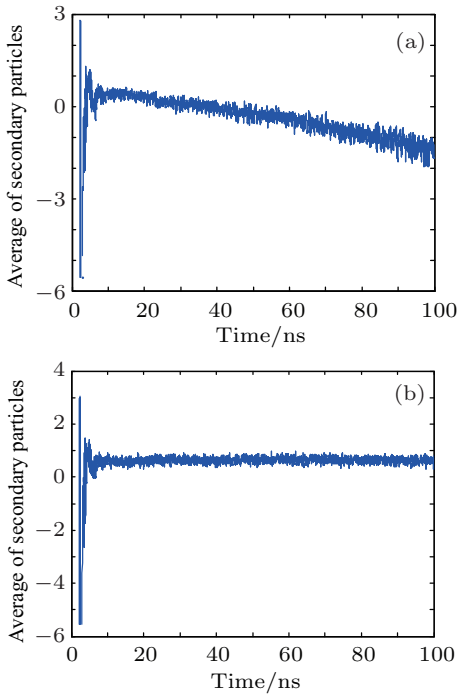


Fig. 12. (color online) Transient evolutions of the secondaries at different input powers: (a) 536 W and (b) 544 W.

Tables 1 and 2 give the convergence analyses of the multipactor simulations. Different meshing criteria are used to perform different simulations. High calculation accuracy of the field distribution in these components can be achieved when the criterion is 20 meshes per wavelength. However, this meshing density is not enough for the multipactor simulation. We find that at least 30 meshes per wavelength and 8 meshes at the narrowest gaps must be set for multipactor simulation of the ridge waveguide filter, which is much more rigorous than the field simulation.

Table 1. Predicted multipactor thresholds at different meshing criteria in the transformer.

The total meshes	5.96×10^5	1.6×10^6
The breakdown threshold/W	1750	1750

Table 2. Predicted multipactor thresholds at different meshing criteria in the filter.

The total meshes	5.5×10^4	7.8×10^4	1.0×10^6	1.5×10^6
The breakdown threshold/W	610	670	544	544

4. Experimental validation

As shown in Fig. 13, a system for measuring the multipactor threshold is developed in a high vacuum chamber. As shown in Fig. 13(b), the test configuration is composed of signal amplifying circuit, reverse and forward coupling circuit, thermal vacuum chamber, and monitoring devices. The forward-reverse power nulling detection method is used in either CW or pulsed mode for multipaction testing.[9] The nulling method is a global detection method, where the incident power to a device under test (DUT) is nulled against the reflected power. A multipaction discharge creates an imbalance leading to a loss of the null, which can be detected by the spectrum analyzer.

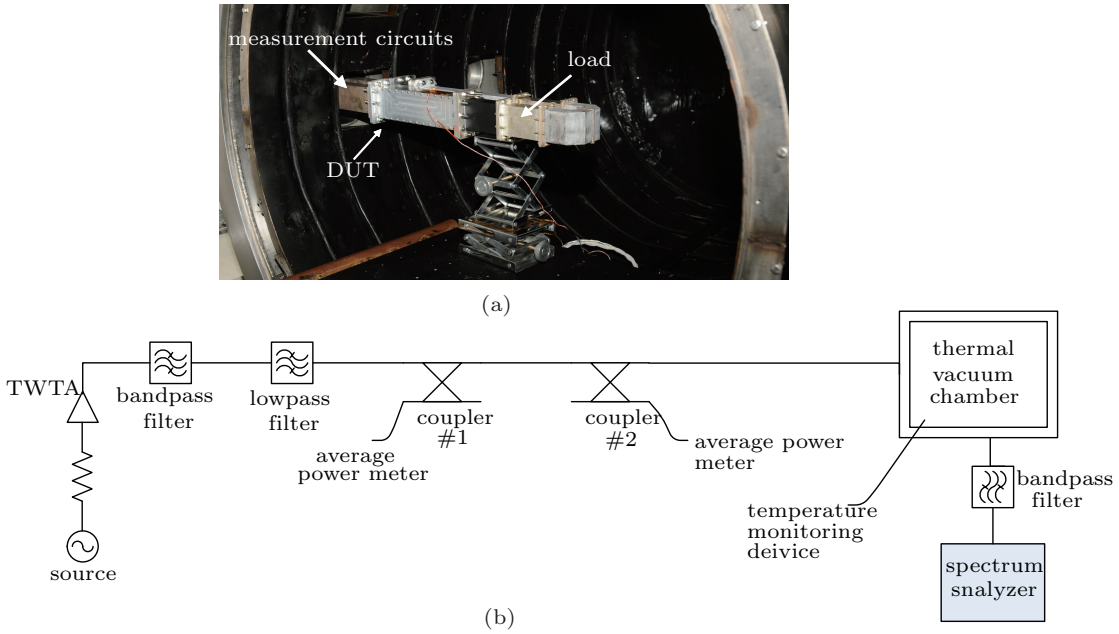


Fig. 13. (color online) Multipactor measurement system.

By such equipment, multipactor measurements are carried out on the impedance transformer and the ridge waveguide filter as shown in Figs. 15 and 16. A base pressure lower than 6.65×10^{-3} Pa should be guaranteed after a minimum of 12-hours vacuum soaking. The tests are performed by applying the lowest power first, and then increasing the power in steps up to the threshold. As the power level approaches the threshold, short bursts of multipactor are detected as shown in Fig. 14.

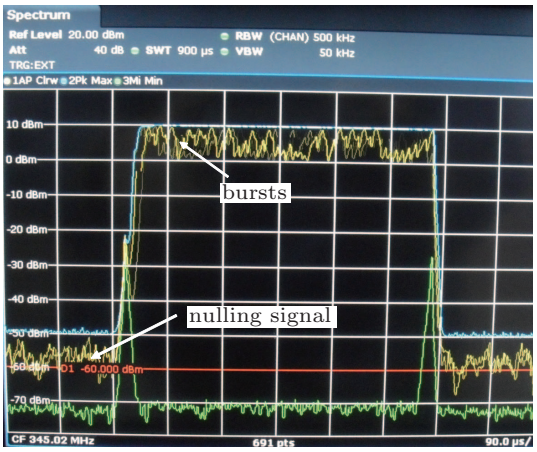


Fig. 14. (color online) Signal waveforms of multipactor discharge.

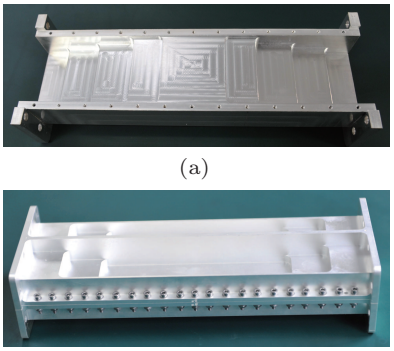


Fig. 15. (color online) Prototypes of the impedance transformer with (a) one piece and (b) assembled device.

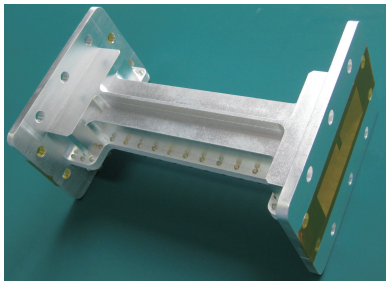


Fig. 16. (color online) Prototype of the ridge waveguide filter.

The thresholds predicted with our method are compared with the experimental data in Table 3. It is clear that the simulation results match well with the experimental data, which therefore validate our simulation method. Besides this, the calculation accuracy is obviously improved compared with that of the multipactor calculator which is based on the parallel approximation and the Monte Carlo method.

Table 3. Multipactor thresholds of the impedance transformer and the ridge waveguide filter.

	The three-dimensional numerical method/W	the multipactor calculator/W	Experiment/W
The impedance transformer	1750	1450	1800
The ridge waveguide filter	544	273	630

5. Conclusion

A three-dimensional and self-consistent numerical method for the simulation of multipactor effect in arbitrary microwave passive components is presented. By combining the FDTD and PIC method, the interaction between fields and electrons is properly modeled, which in turn makes the predicted threshold of multipactor more accurate than that of the traditional method in which the parallel approximation is used. Besides this, the SEY curve from the Vaughan model is fitted by the measured data, which leads to results closer to those in practice. In order to validate our method, the typical microwave components, the impedance transformer, and the ridge waveguide filter are studied. The simulation results accord well with the experimental data, which demonstrate the accuracy of the method.

References

[1] Vaughan J R M 1988 *Multipactor. IEEE Trans. Electron Dev.* **ED-35** 1172

[2] Zhu F, Proch D and Hao J K 2005 *Chin. Phys.* **14** 494

[3] Lu Q L, Zhou Z Y, Shi L Q and Zhao G Q 2005 *Chin. Phys.* **14** 1465

[4] Woode A and Petit J 1990 *ESA Journal-European Space Agency* **14** 467

[5] Rozario N and Lenzing H 1994 *IEEE Trans. MTT* **42** 558

[6] Vahedi V and Surendra M 1995 *Comput. Phys. Commum.* **87** 179

[7] Fan J Q and Hao J H 2011 *Chin. Phys. B* **20** 068402

[8] Liu Z L, Zhang X F, Yao K L, Wei H L and Huang Y M 2004 *Chin. Phys.* **13** 2115

[9] ESA-ESTEC 2003 *Space Engineering: Multipacting Design and Test*. ESA Publication Division, the Netherlands, ECSS-20-01A

[10] Vicente C, Mattes M, Wolk D, Mottet B, Hartnagel H L, Mosig J R and Raboso D 2005 *Proc. IEEE MTT-S Int. Microw. Symp. Dig.* p. 1055

[11] Kossyi I A, Luk'yanchikov G S, Semenov V E, Zharova N A, Lisak M and Puech J 2010 *Appl. Phys.* **43** 345206

[12] Frotanpour A, Dadashzadeh G, Shahabadi M and Gimeno B 2011 *IEEE Trans. Electron Dev.* **58** 876

[13] Rasch J, Semenov V E, Rakova E, Anderson D, Johansson J F, Lisak M and Puech J 2011 *IEEE Trans. Plasma Sci.* **39** 1786

[14] Semenov V E, Rakova E I, Sazontov A G, Nefedov I M, Pozdnyakova V I, Shereshevskii I A, Anderson D, Lisak M and Puech J 2009 *J. Phys. D: Appl. Phys.* **42** 205204

[15] Chang C, Huang H J, Liu G Z, Chen C H, Hou Q, Fang J Y, Zhu X X and Zhang Y P 2009 *J. Appl. Phys.* **105** 123305

[16] Hockney R W and Eastwood J W 1981 *Computer Simulation Using Particles* (New York: McGraw-Hill)

[17] Eastwood J W 1991 *Comput. Phys. Commun.* **64** 252

[18] Goplen B, Ludeking L, Smithe D and Warren G 1995 *Comput. Phys. Commun.* **87** 54

[19] Liu G Z and Shao H 2003 *Chin. Phys.* **12** 204

[20] Liu L, Li Y D, Wang R, Cui W Z and Liu C L 2013 *Acta Phys. Sin.* **62** 025201 (in Chinese)

[21] Kossyi I A, Luk'yanchikov G S, Semenov V E, Zharova N A, Anderson D, Lisak M and Puech J 2010 *J. Phys. D: Appl. Phys.* **43** 345206

[22] Semenov V E, Zharova N, Udiljak R, Anderson D, Lisak M and Puech J 2007 *Phys. Plasmas* **14** 033509

[23] Li Y and Cui W Z 2012 *Proc.* 42*nd European Microwave Conference*, 29 October, 2012, Amsterdam, The Netherlands, p. 920

[24] Taflove A and Hagness S C 2000 *Computational Electrodynamics: The Finite-Difference Time-Domain Method*, 2nd edn. (Norwood: Artech House)

[25] Yee K S 1966 *IEEE Trans. Antennas Propag.* **14** 302

[26] Zhang H B, Hu X C, Wang R, Cao M, Zhang N and Cui W Z 2012 *Rev. Sci. Instrum.* **83** 066105

[27] Pimpec F L, Kirby R E, King F and Pivi M 2005 *Nucl. Instrum. Methods Phys. Res. A* **551** 187